RESEARCH ARTICLE

VOLCANICA

Lava flow hazard assessment on Bioko Island (Equatorial Guinea): A probabilistic approach using Q–LavHA

Jacob Brauner*[α], Magdalena Oryaëlle Chevrel[β,γ,δ], Thomas R. Walter[ε], Oscar A. N. Ela[ζ], Christine R. Sealing[α,η], and Loÿc Vanderkluysen[α]

[α]Drexel University, 3141 Chestnut Street, Philadelphia, PA 19104, USA.
[β]Université Clermont Auvergne, CNRS, IRD, OPGC, Laboratoire Magmas et Volcans, F-63000 Clermont-Ferrand, France.
[γ]Observatoire volcanologique du Piton de la Fournaise, Institut de physique du globe de Paris, 97418, La Plaine des Cafres, France.
[δ]Université Paris Cité, Institut de physique du globe de Paris, CNRS, 75005 Paris, France.
[ε]GFZ German Research Centre for Geosciences, Telegrafenberg, 14473 Potsdam, Germany.
[ζ]Universidad Nacional de Guinea Ecuatorial, Malabo, Equatorial Guinea.
[η]Research Corporation of the University of Hawai'i, Honolulu, Hawai'i, USA.

Submitted: 2024-05-04 | Accepted: 2025-03-31 | Published: 2025-06-19

Editor: J. Farquharson | Typesetter: J. Farquharson

Abstract

Lava flows are the primary volcanic hazard on basaltic volcanoes, such as those of Bioko Island (Equatorial Guinea). The last eruption on Bioko occurred in 1923, and current emissions of CO_2 indicate the presence of magma at depth and the potential for future activity. Yet, lava flow hazards associated with these volcanoes have not been assessed. Using the probabilistic Q–LavHA model, we create a series of lava hazard maps based on a 12 m resolution TanDEM-X digital elevation model. To constrain the lava flow length parameter, we map seven flows ranging from 2 to 12 km in length, including the reconstructed 1923 lava flow. We constrain the flow elevation corrective factors through field observations to 2–8 m. Based on 436 mapped vents, we calculate a kernel density estimation and use it to weight the probability of vents opening in a given location. The highest vent opening probabilities coincide with increased lava inundation probabilities and are located along the main rift zones of the volcanoes, where the highest density of existing lava sources are found (e.g. cinder cones). Important infrastructure, including the capital city of Malabo, are mostly located in coastal areas with relatively low lava inundation probabilities. Simulated lava pathways follow erosional incisions, with a channeling effect that becomes less pronounced with increasing flow thickness. Simulated lava flows are often redirected by structural features such as the summit graben at Pico Basilé.

Resumen

Los flujos de lava son el principal peligro volcánico en los volcanes basálticos, como los de la Isla de Bioko (Guinea Ecuatorial). La última erupción en Bioko ocurrió en 1923, y las emisiones actuales de CO_2 indican la presencia de magma a profundidad y el potencial de actividad futura. Sin embargo, los peligros asociados con los flujos de lava en esta isla volcánica no se han evaluado. Utilizando el modelo probabilístico Q–LavHA, proponemos una serie de mapas de peligro de los flujos de lava basados en un modelo digital de elevación con resolución de 12 m, obtenido con TanDEM-X. Para restringir el parámetro de longitud del flujo de lava, mapeamos siete flujos que varían de 2 a 12 km de longitud, incluyendo la longitud supuesta del flujo de lava emitido en 1923. Restringimos los factores correctivos del espesor de los flujos mediante observaciones de campo a 2–8 m. Basándonos en 436 conos de escoria mapeados, calculamos una estimación de densidad de conos y la utilizamos para ponderar la probabilidad de la ubicación de las futuras bocas eruptivas. Las probabilidades más altas de apertura de bocas eruptivas coinciden con mayores probabilidades de inundación por lava y se localizan a lo largo de las principales zonas de rift de los volcanes, donde se encuentra la mayor densidad de fuentes de lava existentes (como los conos de escoria). Infraestructuras importantes, incluida la ciudad capital de Malabo, se encuentran mayormente en áreas costeras con probabilidades relativamente bajas de inundación por lava. Las trayectorias de lava modelizadas siguen las incisiones erosionales, con un efecto de canalización que se vuelve menos pronunciado con el aumento del espesor del flujo. Los flujos de lava simulados a menudo son redirigidos por características estructurales como el graben del summit en el Pico Basilé.

Keywords: Lava hazard mapping; Vent opening probabilities; Probabilistic lava modeling; Lava pathway controls.

1 Introduction

Volcanic oceanic islands are edifices typically formed by the buildup of low-viscosity basaltic lava flows from repeated eruptions, often interspersed with layers of pyroclastic material, and structurally influenced by volcano-tectonic deformation processes. As a consequence, although lava is the primary volcanic hazard on such islands, other common processes are significant, such as flank instability, spreading, and dike intrusions as demonstrated by recent eruptions of e.g. Mt. Karthala (the Comoros, 2007), Pico de Fogo (Cape Verde, Portugal, 2015), Cumbre Vieja (the Canary Islands, Spain, 2021), Piton de la Fournaise (La Réunion, France, 2022), Kīlauea (Hawai'i, USA, 2023), the fissure eruptions near Grindavík (Iceland, 2024), and La Cumbre (Galápagos, Ecuador, 2024).

Although remotely sensed imagery and easily applicable models are readily available, volcanic hazards are often insufficiently assessed for many volcanic regions. For example, Bioko (Equatorial Guinea, Figure 1) is a volcanic island that consists of three coalescent volcanoes: Pico Basilé, Pico Biaó, and Gran Caldera de Luba. The last documented erup-

*jb4356@drexel.edu

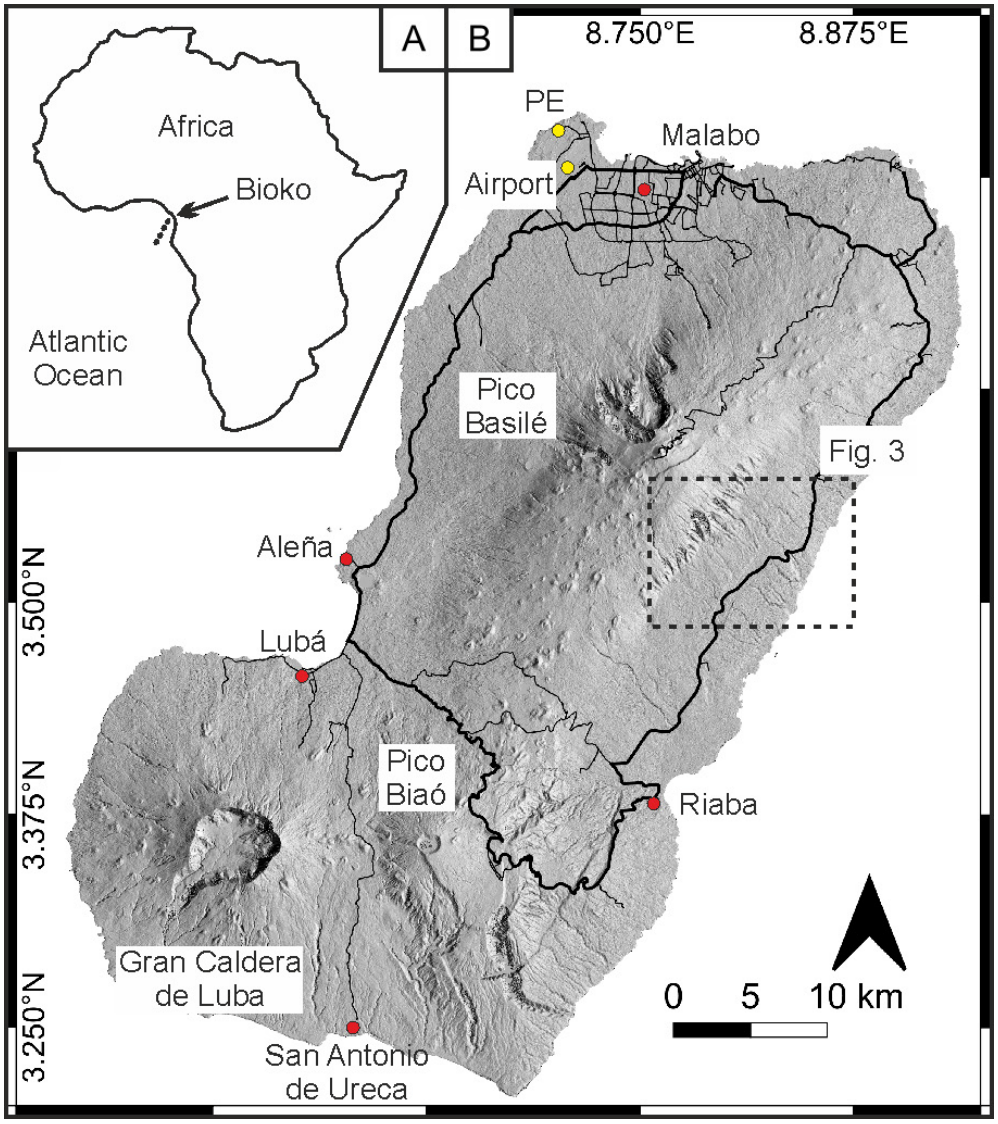

Figure 1: Bioko Island. [A] Inset showing the location of Bioko Island relative to Africa. [B] Shaded relief map of Bioko Island highlighting the NE-SW structurally elongated shape and location of the three main volcanic edifices (Pico Basilé, Pico Biaó, and Gran Caldera de Luba), major cities (red dots), critical infrastructure (yellow dots) such as the international airport and the Punta Europa LNG terminal (PE), and roads (black lines). The dash-lined box outlines the location of Figure 3. Based on a digital elevation model from TanDEM-X.

tion occurred in 1923 at Pico Basilé [*Enciclopedia universal ilustrada europeo americana* 1924]. The three volcanoes are part of the Cameroon Volcanic Line (CVL). Other volcanoes of the CVL, and in particular Mt. Cameroon (Cameroon), erupted effusively multiple times over the last decades, with the last eruption occurring in 2000 [Suh et al. 2003; Bonne et al. 2008; Njome et al. 2008; Thierry et al. 2008]. In contrast to Mt. Cameroon [Favalli et al. 2012], the lava flow hazards for the volcanoes on Bioko have never been assessed, although there are indicators that the system is still active. Volcanic gas (CO_2) is being emitted at multiple sites all over the island [Sealing 2023]. Furthermore, there are eyewitness reports of a steaming event affecting multiple craters at the summit of Pico Basilé in 2012. The majority of the island's 340,000 inhabitants live in the capital city of Malabo (Figure 1B), close to the active volcanoes, highlighting the need for a hazard assessment.

To assess lava flow hazards, probabilistic models can be used to create hazard maps showing the lava inundation probabilities for a given area unit. Such maps are important tools for guiding eruption response management and risk mitigation. Over time, a variety of models were successfully employed for several highly active basaltic volcanoes. Models based on steepest descent algorithms like `DOWNFLOW` [Favalli et al. 2005], `Q–LavHA` [Mossoux et al. 2016], and `MrLavaLoba` [de' Michieli Vitturi and Tarquini 2018] were used to create hazard maps for Mt. Etna in Italy [Favalli et al. 2009b; de' Michieli Vitturi and Tarquini 2018], Pico de Fogo [Richter et al. 2016], Piton de la Fournaise [Chevrel et al. 2021], Mt. Karthala [Mossoux et al. 2019], Mt. Cameroon [Favalli et al. 2012], Kīlauea [de' Michieli Vitturi and Tarquini 2018], Paricutìn in Mexico [Becerril et al. 2021], Fagradalsfjall in Iceland [Pedersen et al. 2023], or Mt. Nyamulagira and Mt. Nyiragongo in the Democratic

Republic of Congo [Favalli et al. 2009a; Kervyn et al. 2024]. Other models based on cellular automata, which describe the distribution of lava on a given surface as a settling process, including GPUFLOW (an evolution of MAGFLOW [Vicari et al. 2007; Del Negro et al. 2008; Cappello et al. 2022]) and Molasses [Connor et al. 2012], have been applied to Mt. Etna [Vicari et al. 2007; Del Negro et al. 2008; Herault et al. 2009; Cappello et al. 2015a], Mt. Aragats in Armenia [Connor et al. 2012], Tolbachik in Russia [Kubanek et al. 2015], and Pico Island in Portugal [Cappello et al. 2015b].

In general, these models simplify lava flow properties to a few parameters, e.g. length, thickness, or volume, and mostly neglect characteristics such as temperature or viscosity. Nevertheless, parameters like lava flow thickness and length indirectly reflect the thermo-rheological properties of lava flows. As basaltic lava cools down, it changes from behaving as Newtonian to a Bingham fluid, and its yield strength is proportional to the thickness of the flow [Hulme 1974; Moore et al. 1978; Pinkerton and Wilson 1994; Chevrel et al. 2013]. Furthermore, yield strength and viscosity are directly linked to the temperature, chemical composition and in particular the silica content, crystal content, and vesicularity [e.g. Shaw 1972; Ryerson et al. 1988; Cashman et al. 1999; Harris and Allen 2008]. The length of basaltic lava flows is primarily controlled by effusion and cooling rates as described by Walker [1973] and Harris and Rowland [2009]. High effusion rates are often observed in the initial phases of an eruption. The rapid advance of the lava allows for relatively long flows before the flow unit ultimately stops advancing due to the coupled decrease in temperature and increase in viscosity. Enhanced thermal insulation (channels, crusts, or tubes) may increase potential flow lengths significantly before reaching its cooling limits, even at decreasing or low effusion rates. Eruptions with low effusion rates typically form short lava flows. Consequently, detailed observations of flow geometries from recent flows are desirable to constrain model input parameters and thus to create realistic hazard maps. No data for lava flow geometries on Bioko are available in the literature.

In addition, probabilistic models such as Q–LavHA must consider vent opening probabilities. In theory, vent density is related to the probability of future vent opening, the higher the density, the higher the probability for a new vent to open up in a given area [Connor and Connor 2009; Bebbington 2013; Connor et al. 2019; Schmidt et al. 2022]. In previous studies, eruptive centers on Bioko have been mapped based on satellite imagery [Tibaldi et al. 2014; Schmidt et al. 2022; Brauner et al. 2024]. The vents are clustering along the volcanic rift zones along the main axis of Pico Basilé and the saddle between Pico Biaó and Gran Caldera de Luba [Brauner et al. 2024]. In this study, we present the first lava flow hazard assessment for Bioko. For this, we estimated the model input parameters (flow length and thickness) based on remotely sensed and field observations. We calculated the vent opening probabilities from the mapped eruptive centers provided by Brauner et al. [2024] to weight simulated lava flows. Using the Q–LavHA model [Mossoux et al. 2016], we created a series of hazard maps to account for the variability of the model input and to test how it potentially affects lava flow pathways. To assess the potential hazards, we identified areas that are likely to be affected by lava with a focus on major cities, settlements, and infrastructure.

2 Study area

The three volcanoes on Bioko Island and Mt. Cameroon form the transition between the continental and oceanic sectors of the NE–SW striking tectono-magmatic alignment of the CVL. Specifically, Pico Basilé is located at the edge of the continental shelf. The alignment extends from Lake Chad in the northeast to the island of Annobón in the southwest [Déruelle et al. 2007] and consists of 13 major volcanoes and more than 1300 monogenetic eruptive centers [Schmidt et al. 2021]. The volcanic activity on the CVL started ~66 Ma on the continental sector and 31 Ma on the oceanic sector [Marzoli et al. 2000; Njome and de Wit 2014].

The island of Bioko itself consists of three coalescing volcanoes and is located at 3° 30’ N and 8° 42’ E in the Gulf of Guinea (Central Atlantic Ocean; Figure 1A). We refer to the volcanoes by their current names, from NE to SW: Pico Basilé, Pico Biaó, and Gran Caldera de Luba (Figure 1B). These used to be known as Santa Isabel, San Joaquin, and San Carlos, respectively, during the Spanish colonial era. Brauner et al. [2024] defined distinctive rift zones striking NE–SW along the long-axis of Pico Basilé, and E–W along the saddle between the two southern volcanoes. Compositionally, volcanic products consist of basalts, hawaiites and mugearites [Yamgouot et al. 2016]. K/Ar age measurements revealed an age <1.33 ± 0.07 Ma for lava flows on Bioko [Hedberg 1969; Aka et al. 2004]). Piper and Richardson [1972] constrain the age range of the island to the Brunhes magnetic chron (< 0.7 Ma) based on a magnetic survey. The last eruption occurred in 1923 CE on Pico Basilé [*Enciclopedia universal ilustrada europeo americana* 1924]. We did not find reports of eruptions of the other two volcanoes.

3 Data and methods

3.1 Data sources

Our morphologic dataset is based on satellite X-band (wavelength 3.1 cm) TerraSAR-X (TSX) / TanDEM-X (TDX) synthetic aperture radar (SAR) data with a nominal resolution of 3 m provided by the German Aerospace Center to investigate volcanic structures and to model probabilistic lava flow hazards on the island of Bioko. Radar signal penetration through the cloud-covered atmosphere is a major advantage of these data and provides gap-free coverage [Rizzoli et al. 2017]. X-band emissions have a relatively short wavelength in the microwave range, and tend to scatter in denser canopy areas as a result [Schlund et al. 2021]. The derived DEM (level 3 product) is part of the TanDEM-X DEM 2020 and was released with a nominal resolution of 12 m, and a vertical accuracy of 2 m for flat terrain and 4 m for slopes greater than 20° [Wessel et al. 2022]. The geomorphological study and lava flow simulations were performed using the full resolution (12 m) digital elevation model.

For modeling, all geospatial data sets are projected in the coordinate reference system EPSG:32632 - WGS 84 / UTM

zone 32N. We used geospatial data from the OpenStreetMap project (OSM 2021) and referenced old maps of the island [Instituto Geográfico Nacional 1981a; b; c; d] to identify relevant places, geographical features such as rivers, and infrastructure. The complete documentation of the performed analysis and files for this study can be found in Supplementary Material 1. Furthermore, we conducted a field campaign to ground-truth our observations in November and December 2022.

3.2 Model and parameters

We assess the hazards of lava flows on Bioko using the probabilistic Q–LavHA model of Mossoux et al. [2016], which is based on the mathematical framework of Felpeto et al. [2001]. We chose Q–LavHA because it is a user-friendly Q–GIS plugin that allows lava flow simulations without requiring high computational power for individual flow simulations. For large numbers of flow simulations as required to produce lava flow hazard maps on a regional scale however, the processing time might still last several weeks or months, depending on DEM resolution and computer capacity.

The model calculates potential lava flow pathways from a given vent following the path of steepest descent on a given DEM. For a single vent it simulates N lava flows of a given length L flowing downhill. Based on the frequency each pixel is invaded by lava, the model calculates the inundation probability with respect to the number of iterations N. The model adds the elevation corrective factor Hc to the topography for the lava-containing pixel, representing the flow's thickness. Another elevation corrective factor, Hp, is added if the lava-containing pixel cannot progress because the immediately surrounding pixels are higher in elevation, and thus prevents flow arrest. The model offers an H16 option that considers the 16 next surrounding pixels if neither the addition of Hc nor Hp allow the lava to propagate further. Therefore, the H16 option resembles the ability of a lava flow to fill up small depressions before progression continues. These topographic corrections are temporary and thus do not affect simulated flows during subsequent iterations. Furthermore, a Monte Carlo algorithm is applied to randomly perturb flow pathways [Felpeto et al. 2001; Mossoux et al. 2016].

The two key parameters for Q–LavHA are the length of the flows, L, and the elevation corrective factor, Hc. To constrain the length, we mapped lava flows on the DEM (see Section 4.1). Accordingly, we decided to create maps for a variable length parameter covering the range of length we measured (Euclidean length, i.e. as-the-crow-flies distance): 3, 7.5, and 12 km.

We constrained the factor Hc, based on the thickness measured on the few accessible lava flows cropping out in the field (see Section 4.1). To evaluate the effect of flow thickness, we created maps for Hc = 2 m, 5 m, 8 m, and Hp = Hc +4 m.

We assessed the effects of the variable flow length (L) and elevation corrective factors (Hc) parameters for simulations of individual case studies, and for the hazard map for the entire island. For individual case scenarios, we simulated N = 1500 flows per vent, while for the large-scale hazard maps, we simulated a vent every dV = 300 m, and N = 500 lava flows per vent.

We weighted the simulated vents based on vent opening probabilities. The probability of future vent opening is determined on the basis of location of historical vents, assuming that future vents are more likely to open in areas where previous vents cluster. Furthermore, the probability of future vent opening should be scaled to the recurrence probability. Indeed, older vents can be masked by subsequent eruptions. However, we do not have sufficient data on the recurrence time for Bioko (see Section 5.1.3 for a detailed discussion) and therefore consider that the probability density function corresponds to the future vent opening probability. For this purpose we ran a Nearest Neighbor Analysis in ArcGIS 10.8.1 on the identified vent locations, where index values < 1 indicate clustering [Le Corvec et al. 2013], and calculated a Kernel Density Estimation (KDE) in SAGA GIS 7.8.2. The resulting probability density function provides an estimate of future vent opening probabilities [Connor and Connor 2009; Bebbington 2013; Connor et al. 2019; Schmidt et al. 2022].

Referring to Connor et al. [2019], the kernel shape has only minor implications on the probability density function so we followed their recommendation and chose a Gaussian kernel function. In order to reduce the computational efforts, we only simulated vents in areas with an opening probability greater than 0.01 %. Schmidt et al. [2022] used the SAMSE (Summed Asymptotic Mean Squared Error) bandwidth estimator and calculated anisotropic bandwidths of 2913 and 3087 m for their KDE for the vents on Bioko. In accordance, we chose a bandwidth of 3000 m for this study. In the next step, we weighted the inundation probabilities for each vent with the PDF at the individual vent locations (pixel) corresponding to the DEM resolution.

4 Results

4.1 Field observations and mapping of lava flows from satellite DEM

Using the DEM (12 m resolution), we were able to identify and track six distinct lava flows from their origin to their termination, serving as a reference dataset (Figure 2A). The length of these flows ranges from 1.9 to 4.0 km (Table 1). Additionally, the 1923 eruption produced a lava flow on the eastern flank of Pico Basilé and continued toward the sea. Although the flow is now covered by dense vegetation and likely progressed through an erosional incision, we had to identify the

Table 1: Length of the mapped lava flow units (1–6) and the 1923 flow as shown in Figure 2 and 3.

Flow number	Length [km]
1	1.9
2	2.7
3	2.3
4	2.8
5	3.8
6	4
1923 flow	~12

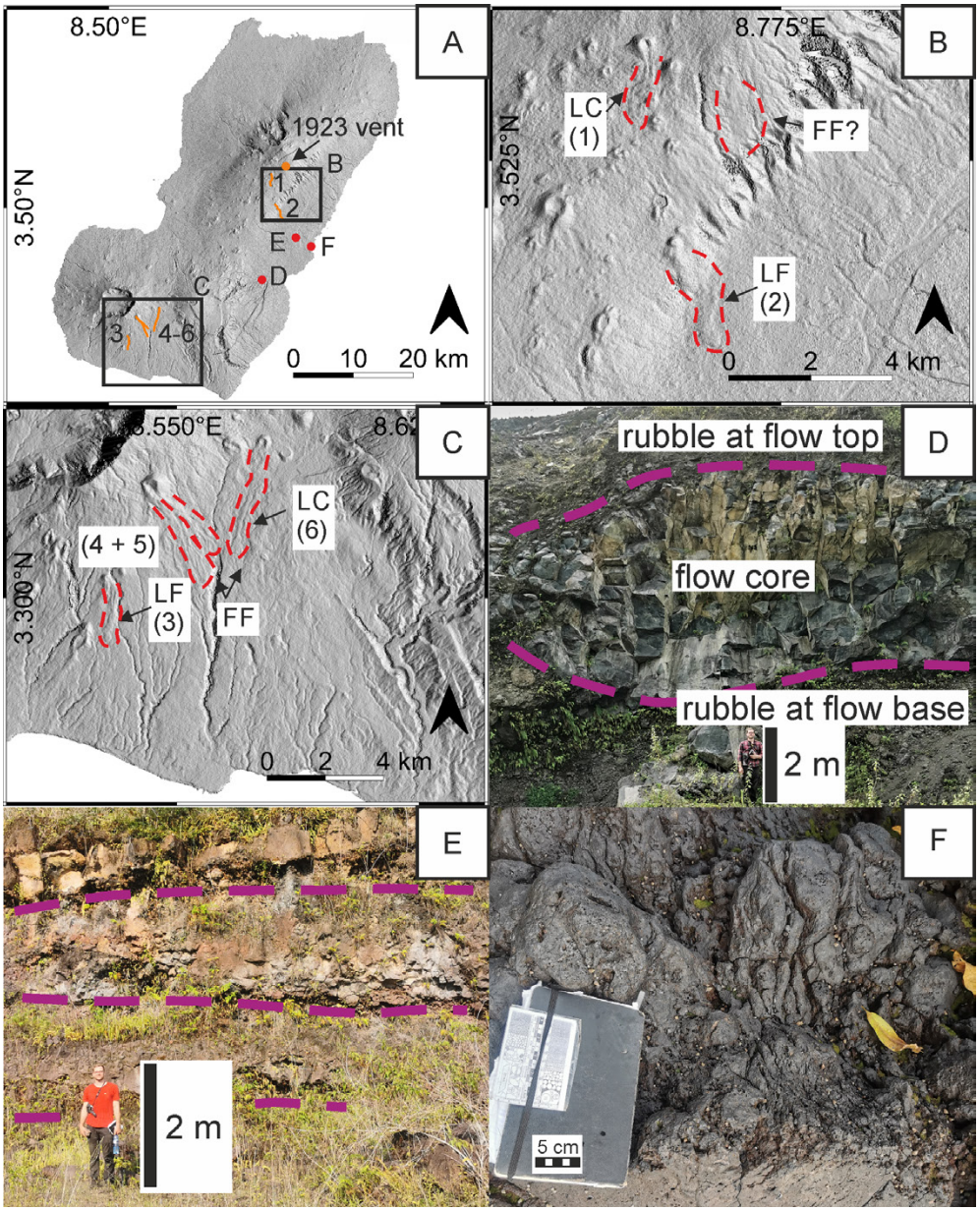

Figure 2: Lava flow mapping and field observations. [A] Overview of lava flow units 1–6 (orange lines), the location of the 1923 vent location (orange dot), and locations of insets [B] and [C], as well as outcrops ([D]–[F]; red dots). [B] Southeastern flank of Pico Basilé including lava flow units #1 and #2, as well as a potential lava flow field (red dashed line); LC: lava channel, LF: Lava flow, FF: Flow field. [C] Southern flanks of Pico Biaó and Gran Caldera de Luba including lava flow units #3–6 (red dashed lines); LC: lava channel, LF: Lava flow, FF: Flow field. [D] Outcrop of an ʻaʻā flow in an active quarry northeast of Pico Biaó. The massive inner part has a thickness of approximately 4–6 m and is surrounded by layers of rubble at the upper and lower boundaries. [E] Outcrop of stacked lava flows in an abandoned quarry southeast of Pico Basilé. Each flow unit is approximately 2 m thick and covered by thin dm-scale layers of rubble. [F] Pāhoehoe lava with ropey surface on a beach southeast of Pico Basilé.

most likely source vent to constrain its length (see Section 4.2). This constraint revealed a flow length of maximum 12 km.

All the lava flows mapped on the DEM are found at the southeastern flank of Pico Basilé (Figure 2B) and at the southern slope of the saddle between the two volcanoes in the south of the island (Figure 2C). Close to the summit of Pico Basilé, several monogenetic cones are breached and show indications of lava flow exiting the cone. Lava flow #1 (Figure 2A, 2B) is 1.9 km long and shows well expressed levees. From crest to crest, the channel has a width of approximately 120 m. To the east, we observed another potential lava flow field but we do not consider it here because it cannot be well outlined (Figure 2B). Flow #2 is located a few kilometers down the flank of Pico Basilé from Flow #1 and has an approximate length of 2.7 km and shows a well expressed lobate termination, but no levees (Figure 2B). South of the caldera of Gran Caldera de Luba, flow unit #3 extends over 2.3 km. The upper half of the flow shows levee structures (~100 m from crest

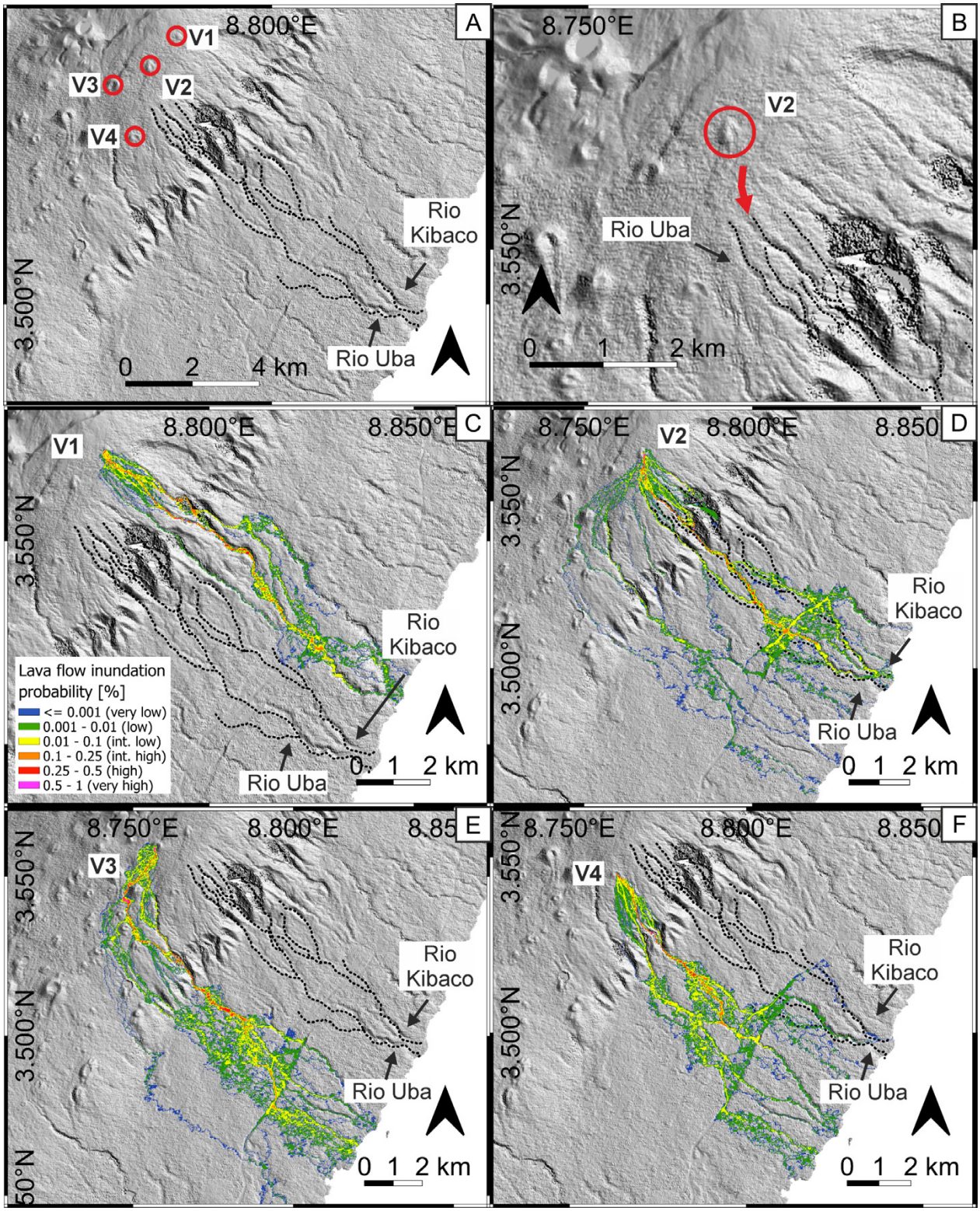

Figure 3: Identification of the 1923 eruptive center at the southeastern flank of Pico Basilé (see Figure 1 for overview). The simulations are based on the 12 m DEM with N = 1500, L = 20 km, Hc = 2 m. [A] Scoria cones V1–V4 (red circles) located upstream of the river gullies of Rio Uba and Rio Kibaco (black dotted lines). [B] Close-up on vent V2; the red arrow indicates the initial pathway of a lava flow towards Rio Uba. [C] Simulation of lava flow paths from vent V1. [D] Simulation of lava flow paths from vent V2, indicating high probabilities for lava flowing down Rio Uba. [E] Simulation of lava flow paths from vent V3. [F] Simulation of lava flow paths from vent V4. Note that the flow path simulations are affected locally by the actual road incision, which was not present in 1923.

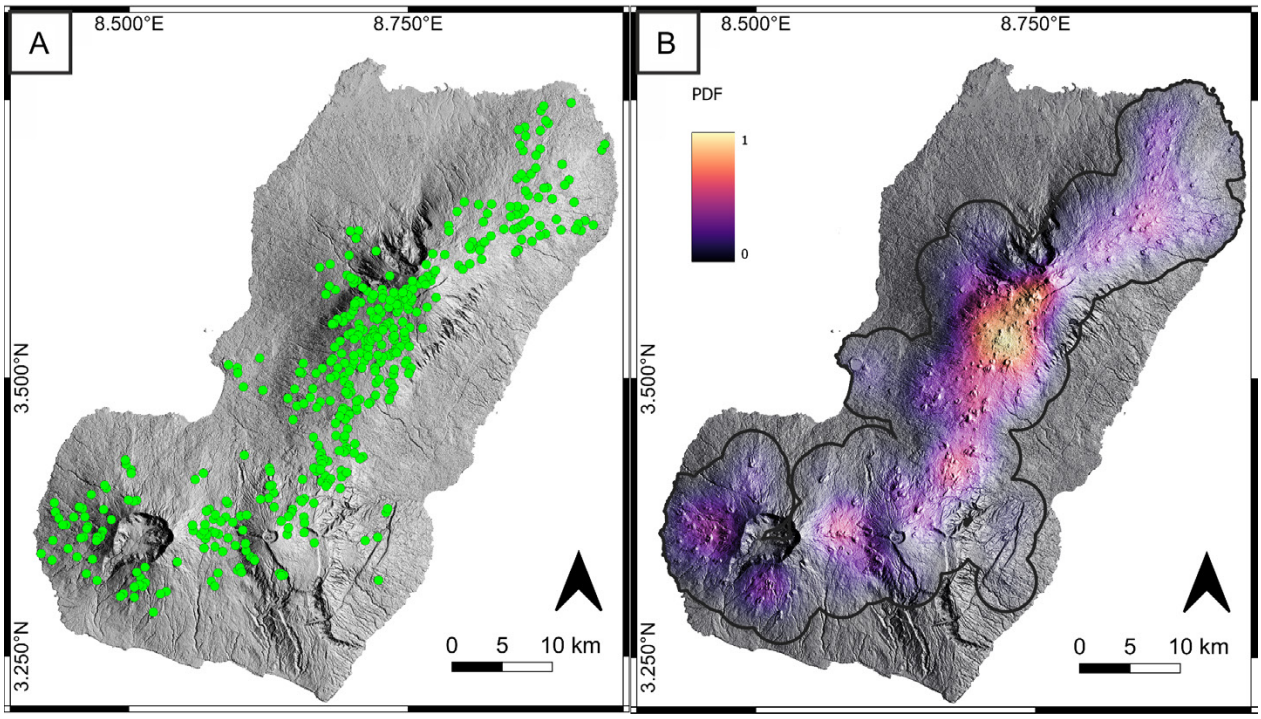

Figure 4: Location of volcanic vents on Bioko, and probabilities of vent opening. [A] Distribution of the 436 vents (shown as green dots) mapped on Bioko. [B] Probability density function (PDF) for the vents as shown in [A], brighter color indicates a higher PDF. The PDF is normalized to 1 and corresponds to the relative vent opening probabilities for the island. The bold black line encloses the area with a vent opening probability greater than 0.01 %. To reduce the computational time, we only simulated vents within this area. However, it is possible that a vent opens outside this area although the probability is low.

to crest) whereas the lower part is compact and has a lobate ending (Figure 2C). At the saddle between Pico Biaó and Gran Caldera de Luba, we observed three individual flow lobes (#4, 5, and 6) ranging from 2.7 to 4.0 km in length. The flows show well expressed channel structures (Figure 2C). During our field campaign, we observed outcrops of lava flows of different types (pāhoehoe and ʻaʻā) and of variable thickness. The flow thicknesses range approximately from 2 to 8 m (Figure 2D, 2E). Thin flow units of about 2 m thickness, separated by decimeter-scale layers of rubble, were often stacked on top of each other (Figure 2E). The thicker ʻaʻā flow reaches a thickness up to 8 m with the massive flow core, 4–6 m thick, sandwiched between top and bottom layers of rubble, 2–4 m each (Figure 2D). Due to the dense vegetation, original surface features like indicators for pāhoehoe lava are rarely preserved. Nevertheless, we found ropey surfaces at two sites close to the seashore southeast of Pico Basilé (Figure 2F).

4.2 The 1923 eruption site

The 1923 eruption produced a lava flow on the eastern flank of Pico Basilé that inundated the area between the rivers of Rio Uba and Rio Kibaco, possibly entering the sea [Sealing 2023]. We identified the rivers Rio Uba and Rio Kibaco in the southeastern sector of Pico Basilé and four potential eruption vents (Figure 3A), hereafter labeled V1, V2, V3, and V4 (Figure 3C–3F).

Using `Q-LavHA`, we modeled lava flow paths for each of these four cones in order to identify the most likely source, by assessing the proximity of the simulated flows to the rivers of Rio Uba and Rio Kibaco for each vent (V1–4). For each scenario, the simulated flows are confined in erosional incisions like the amphitheater-shaped valleys and gullies that can be found on the flanks of Pico Basilé. Although the simulated flow patterns fan out with increasing distance from the vent, for each scenario, there are one or two major gullies that show significantly increased inundation probabilities. Only the simulations from vent V2 (Figure 3B, 3D) allow the majority of simulated paths to flow within the boundaries of the rivers of Rio Uba and Rio Kibaco (Figure 3D). The V2 vent simulations mostly follow the course of the Rio Uba. A second branch of simulated paths heads southwestwards before flowing downslope. On closer inspection, the V2 vent breaches northwards and appears to be feeding lava to the headwater of the Rio Uba (Figure 3B, 3D). From this, we conclude that vent V2 was the most likely source of the 1923 lava flow. To be able to reach the sea, we measured a flow length of approximately 11.9 km.

4.3 Vents and probability density function

Brauner et al. [2024] identified 436 vents from the monogenetic cones distributed over Bioko. Complex monogenetic cones may comprise multiple vents. The majority of vents are located on Pico Basilé with 287 vents across 1107 km^2 (0.26 vents km^{-2}), followed by Gran Caldera de Luba with 77 vents across 412 km^2 (0.18 vents km^{-2}), and Pico Biaó with 73 vents across 423 km^2 (0.17 vents km^{-2}). We find that vents approximately align in NE–SW along the main rift at Pico Basilé, and

in E–W along the ridge between Pico Biaó and Gran Caldera de Luba (Figure 4A). A nearest neighbor analysis with an index of 0.48 confirms clustering for the vents on Bioko (values <1 are interpreted as being clustered, as the average observed distance to the nearest neighbor is lower than that distance predicted from a random distribution). This is reflected in the vent density analysis (Figure 4B). The probability density function (PDF) here corresponds to the vent opening probability acting as a proxy for the spatial variation in eruption probability. For a detailed discussion of the limitations of this assumption, we refer to Section *5.1.3*.

We observe the highest vent opening probabilities (Figure 4B) southwest and around the summit of Pico Basilé. Other areas with increased probabilities are located along the shallow slopes in the northeastern and southwestern sectors of Pico Basilé, and around the central caldera of Gran Caldera de Luba. The area around Malabo (northwestern part of the island), as well as the southeastern flanks of Pico Basilé and Pico Biaó, show very low vent density and hence low vent opening probabilities. We did not find any vents within the two craters / calderas at Pico Biaó and Gran Caldera de Luba, although they likely were the locus of eruptive activity in the past, but are now located in densely vegetated regions that may perturb the radar signal (see Section *5.1.1*).

4.4 Hazard maps

The purpose of the produced maps is to assess potential hazards and not to predict future eruptions nor to evaluate the risks. The intended use of the maps is long-term hazard mitigation. These lava inundation probability maps express the likelihood of lava invasion over the entire island for a potential future eruption. We emphasize that, for a future eruption, the vent opening probability becomes 100 % for the actual eruption site once the eruption has started and a vent has opened, and 0 % for the rest of the island. All maps and datasets are available online (see Data availability) in high resolution.

To build the hazard maps, we simulated lava flow paths from areas with a PDF value >0.0001, which equals a vent opening probability of 0.01 % which represents 1226 km^2 (Figure 4B). We considered a vent every 300 m (1 vent / 0.09 km^2), which resulted in a total of 13622 simulated vents. Given the limited availability of data to constrain the input parameters further (for a detailed discussion see Section 5), we chose to present a reference hazard map using an averaged set of input parameters: L = 7.5 km, Hc = 5 m, and Hp = 9 m (Figure 5). Next, to test the effect of the input parameters (length and elevation corrective factors), we build other lava flow hazard maps for: 1) Hc = 2 m, Hp = 6 m, L = 3 km (Figure 6A); 2) Hc = 8 m, Hp = 12 m, L = 3 km (Figure 6B); 3) Hc = 2 m, Hp = 6 m, L = 12 km (Figure 6C); and 4) Hc = 8 m, Hp = 12 m, L = 12 km (Figure 6D).

In general, we observe the highest lava flow inundation probabilities inside the deeply incised gullies cutting into the flanks and the saddles between the three volcanoes (labeled Pico Basilé, Pico Biaó, and Gran Caldera de Luba in Figure 1). However, we also observe a strong structural control on lava flow pathways. For example, the graben faults at the summit of Pico Basilé block and redirect flows (Figure 5, 6, and 7) and thus the flank sections directly adjacent to the northwest and southeast show only low inundation probabilities. Similarly, the concentric faults around the summit of Pico Biaó act as barriers and thus the southeastern tip of the island is not invaded by any flows.

The areas with high vent opening probabilities show intermediate lava flow inundation probabilities (Figure 4, 5, and 6). This includes the main rift zone at Pico Basilé, and the saddles between Pico Biaó and the other two volcanoes (Figure 4, 5, and 6). For the hazard maps for short lava flows (L = 3 km), these rift and saddle zones are the areas with the highest hazard classes (intermediate). Furthermore, monogenetic cones act as obstacles. The simulated flows circumvent the cones, and in the areas of high cone densities (e.g. rift zones), flows are sometimes confined and channelized between multiple cones, indicated by intermediate to high inundation probabilities. The summit areas of Pico Biaó and Gran Caldera show low probabilities of lava inundation.

As the length of the simulated flows increases, more distal areas are possibly affected. Most cities, villages, and infrastructure on Bioko are located in coastal areas (Figure 1). For the simulations with L = 3 km (Figure 6A, 6B) the coastal regions northwest and southeast of Pico Basilé, as well as the city area of Malabo, except for the eastern outskirts, are largely unaffected by lava. However, simulations for flows with L = 12 km (Figure 6C, 6D) show inundation probabilities greater than zero for most coastal areas. Again, the highest probabilities (high–very high) are found within erosional incisions. Areas adjacent to such major gullies are forecast to be less affected by lava. This indicates a channelizing effect of those gullies. In contrast, relatively flat areas show rather homogenous probability distributions. For example the eastern part of Malabo is incised by gullies, and with increased flow lengths (L = 12 km) these channels are frequently invaded by lava flow simulations. The western part of the city is relatively flat and shows homogeneously, low inundation probabilities. In particular, the northwestern part, including the international airport and the Punta Europa LNG (liquid natural gas) terminal, is very unlikely to be affected by lava according to our simulations.

With increasing flow elevation corrective factor, the observed channelizing effect of the gullies decreases. Simulations for low flow elevation corrective factors (Hc = 2 m; Figure 6A, 6C) show significantly lower inundation probabilities in adjacent areas of deep erosional incision than simulations of thicker flows (Hc = 8 m; Figure 6B, 6D). In particular, the coastal areas of the central part of the island are affected by the simulations of thicker flows (Hc = 8 m; Figure 6D). In those coastal areas, the probabilities rise from mostly none to low, to dominantly intermediate. The bay at Riaba and the bay between Aleñá and Lubá are most likely affected by lava flows from the saddle between Pico Basilé and Pico Biaó, depending on if the lava flows east or west. Similarly, potential eruptions at the saddle between Pico Biaó and Gran Caldera de Luba may produce lava flows that block the supply roads to San Antonio de Ureca or Lubá. In particular, the city of Lubá is located at the outlet of a gully and thus might be impacted by potential lava flows from Gran Caldera de Luba, although

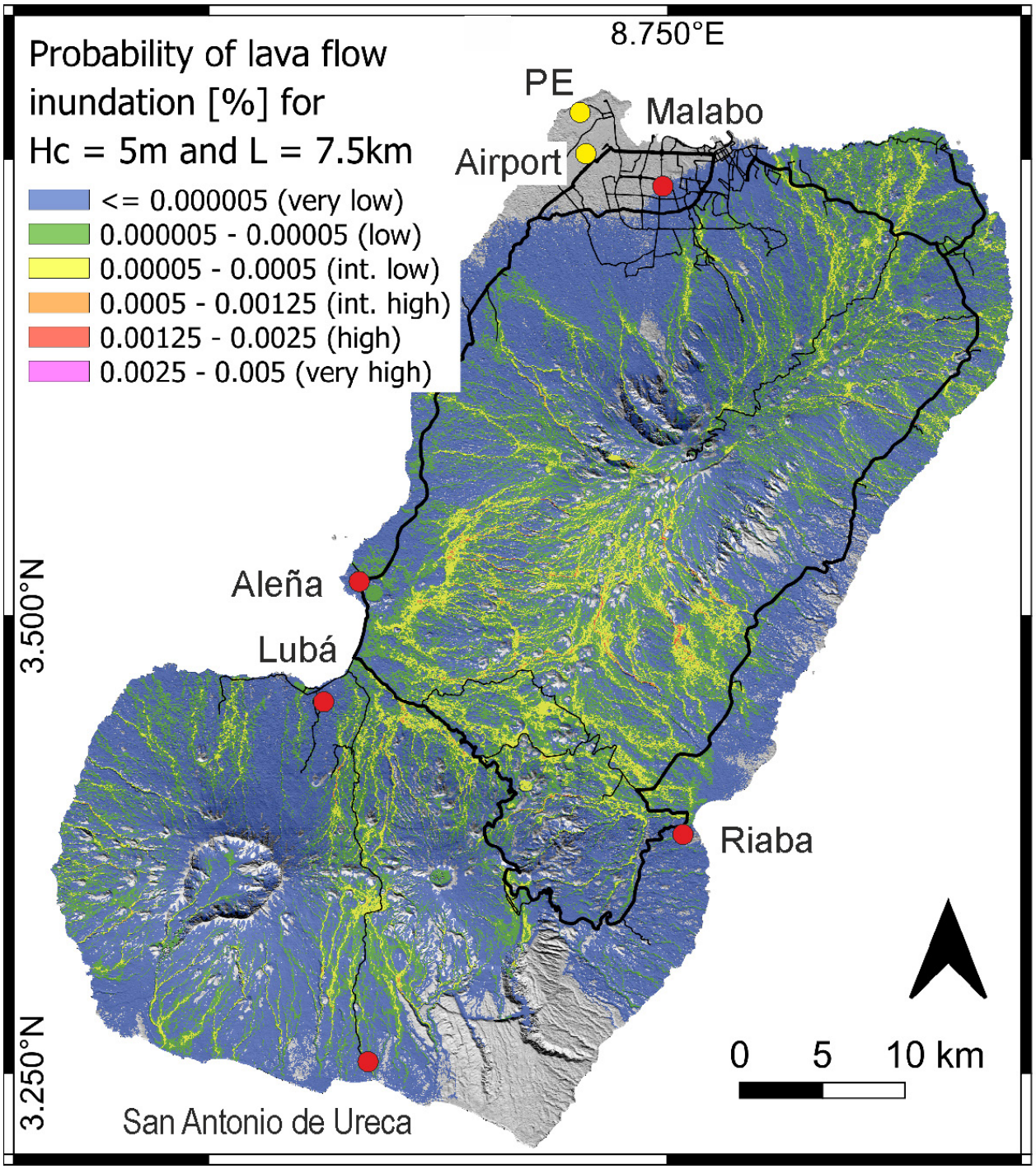

Figure 5: Reference map of lava flow inundation probabilities on Bioko Island for lava flows for an averaged set of parameters, with *L* = 7.5 km, *Hc* = 5 m, and *Hp* = 9 m. Red dots: major cities; Yellow dots: critical infrastructure such as the international airport and the Punta Europa LNG terminal (PE); Black lines: roads.

the overall probability for this scenario is low. The area east and southeast of Aleñá shows the most significant increase of pixels changing to high probabilities of lava flow invasion (Figure 6D) while the inundation probabilities further uphill remain almost constant. East of Aleñá, the number of simulated flows from multiple upslope vents overlap more often at greater distance from the simulated vents and thus accumulate in relatively flat areas, being blocked and redirected by fault structures. With an increasing flow elevation corrective factor, a growing number of flows overlap, resulting in elevated lava invasion probabilities. We did not observe this effect at the graben structures on the opposing (SE) flank of Pico Basilé. There, the graben faults are repeatedly incised by erosion.

For the simulated vent at the summit of Pico Basilé (Figure 7), two major effects can be observed. First, the flows are being blocked and redirected by the northeastern summit

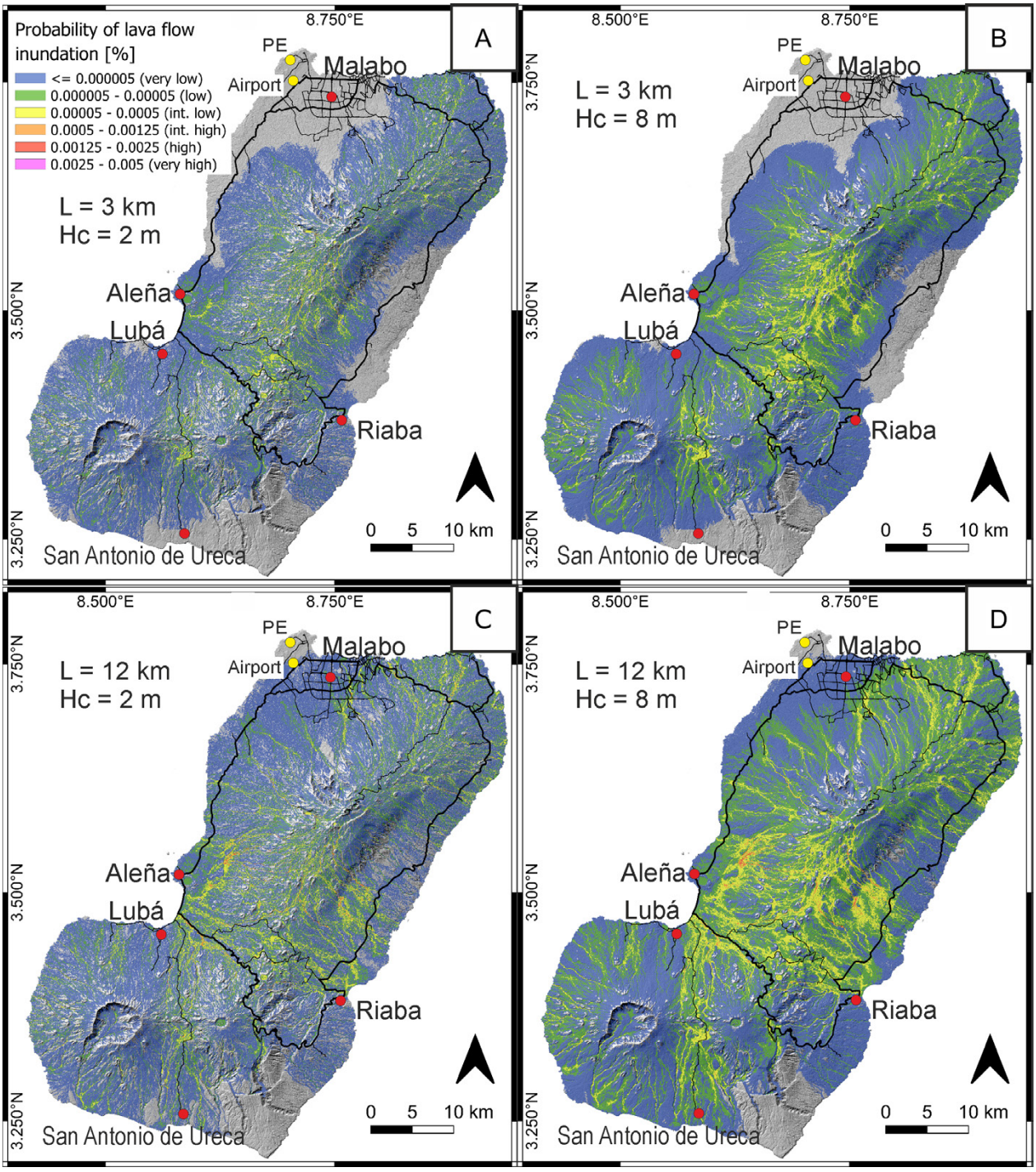

Figure 6: Variability of the lava flow inundation probabilities on Bioko Island for different length parameters and lava flow elevation corrective factors. [A] Hazard map with *L* = 3 km, *Hc* = 2 m, and *Hp* = 6 m. [B] Hazard map with *L* = 3 km, *Hc* = 8 m, and *Hp* = 12 m. [C] Hazard map with *L* = 12 km, *Hc* = 2 m, and *Hp* = 6 m. [D] Hazard map with *L* = 12 km, *Hc* = 8 m, and *Hp* = 12 m. To validate the effect of features such as erosional incisions and faults on the lava flow paths and the created hazard maps, we present simulations for a single hypothetical eruption vent above the graben fault at the summit of Pico Basilé with a length parameter that allows the flows to reach the sea and varying elevation corrective factors (Figure 7). Red dots: major cities; Yellow dots: critical infrastructure such as the international airport and the Punta Europa LNG terminal (PE); Black lines: roads.

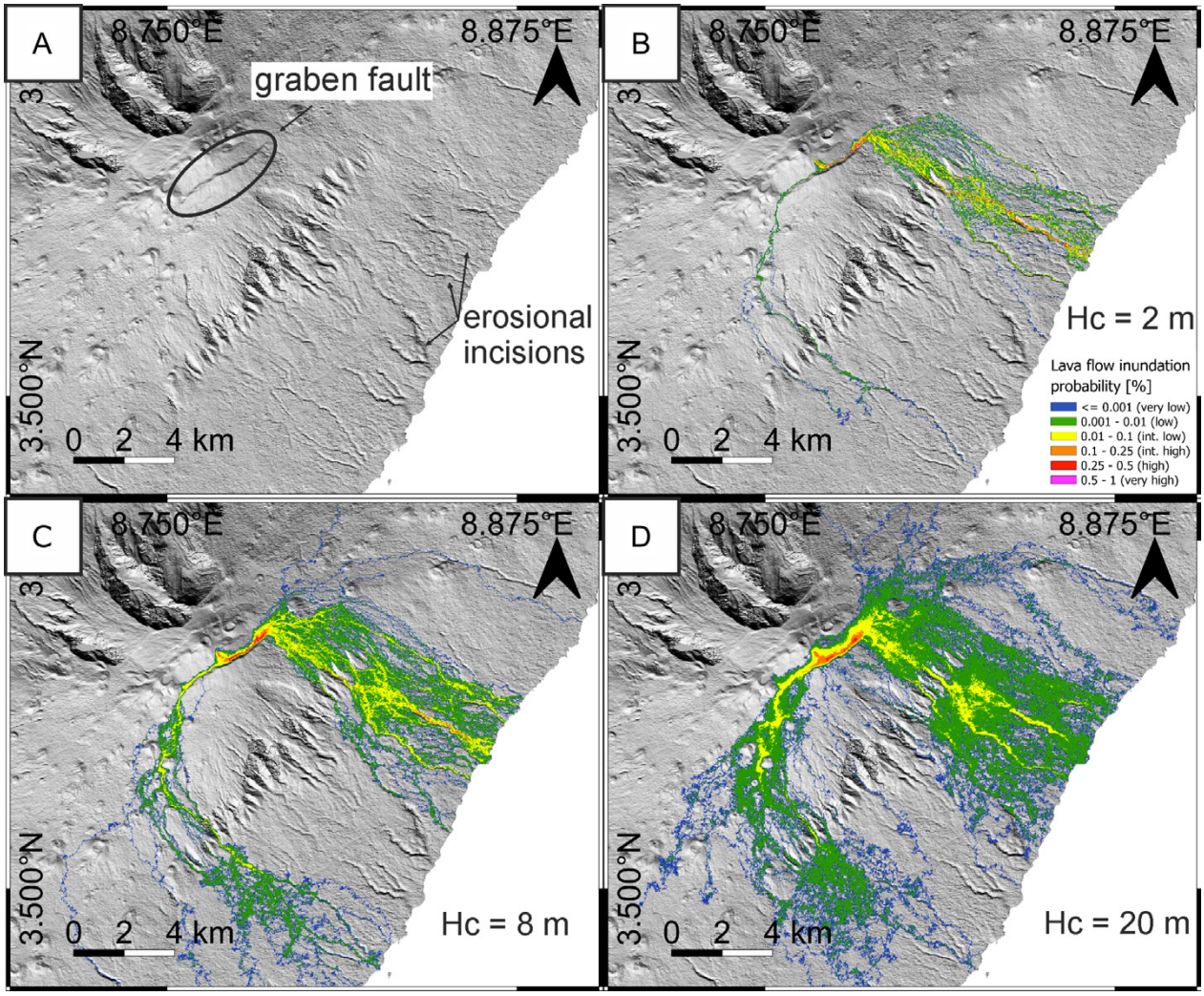

Figure 7: Simulation of a single vent at the summit of Pico Basilé with lava flows with a length that allowed the flows to reach the sea and varying elevation corrective factors, where *H*p = *H*c +4 m. [A] Topographic features, such as faults and erosional incisions at the southeastern flank of Pico Basilé. [B] For *H*c = 2 m, the majority of flows are being redirected by the southeastern graben fault and channelized into erosional incisions. [C] Flows with *H*c = 8 m are being less easily channelized in gullies, and thus more likely to inundate adjacent areas. [D] First lava flows are able to overcome the graben fault at *H*c = 20 m. Further downslope, the erosional incisions are still showing the highest inundation probabilities, but large areas adjacent to the gullies show inundation probabilities greater than zero.

graben fault, which has an offset of 50–70 m. The majority of simulated flows are channelized northeastwards along the graben fault, indicated by high to very high inundation probabilities. The other flows head towards the southwest. Once the flows bypassed the fault, they mostly follow erosional incisions along the southeastern flank of Pico Basilé, on the map indicated by intermediate to high probabilities. With increasing *H*c parameters, the distribution of simulated flows fans out. Gullies still have the highest inundation probabilities but a higher number of simulated flows follow pathways outside of the gullies. Very high *H*c values (20 m and more, Figure 7D) allow individual flows to overcome the graben fault.

In conclusion, with an increasing flow elevation corrective factor, simulated flows can overcome larger topographic obstacles. As the flow elevation corrective factors increase, the simulated flows are still channeled by deeply incised gullies. However, shallow gullies have less potential to channelize flows, and therefore the area that has an inundation probability higher than zero is larger for thicker flows.

5 Discussion

5.1 Limitations

5.1.1 *Model uncertainties due to vent and lava flow inventories*

Although remote sensing techniques, such as satellite-based radar, allow investigations of areas that may not be easily accessible, certain limitations such as geometric distortions and vegetation have to be considered. Geometric distortions were corrected by the German Aerospace Centre (DLR) in order to generate the DEM, but resulted in a decrease of the spatial resolution from 3 to 12 m per pixel.

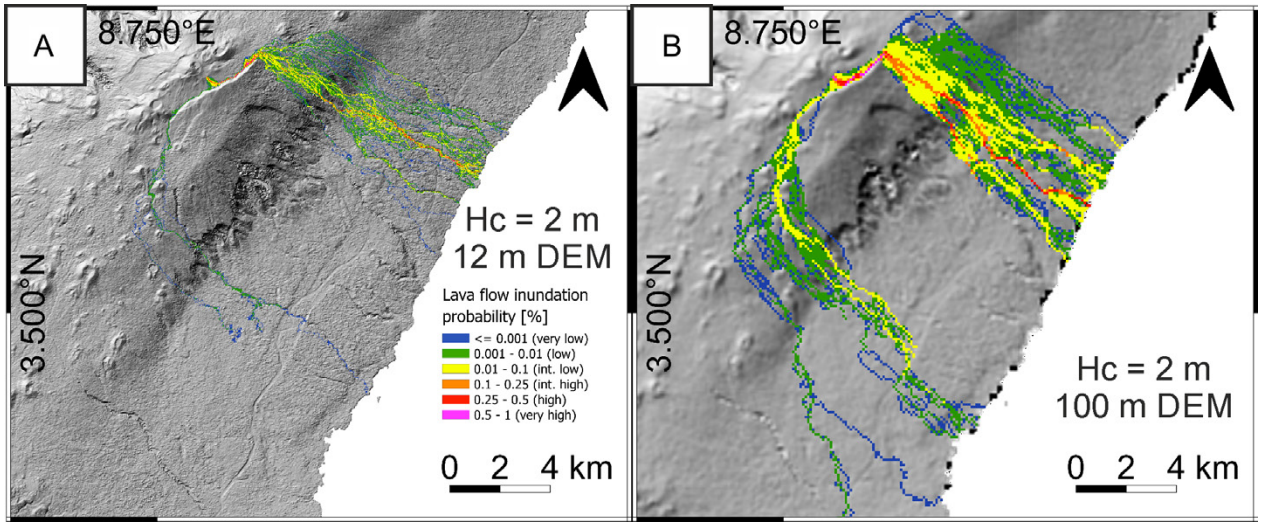

Figure 8: Simulation of a single vent at the summit of Pico Basilé with lava flows with a length that allowed the flows to reach the sea and fixed elevation corrective factors of *Hc* = 2 m and *Hp* = 6 m on [A] a DEM with 12 m resolution and [B] a DEM with 100 m resolution.

The vertical resolution of 2 m for flat terrain and 4 m for slopes greater than 20° is strongly affected by the dense vegetation on Bioko [Wessel et al. 2022]. X-band radar waves allow penetration through canopy only to a certain degree. The resulting vertical offset for tropical rain forests such as that of Bioko can be up to 10 m or more [Tanase et al. 2015; Grohmann 2018]. Therefore, volcanic features like lava flows and monogenetic cones might be obscured on the DEM. Information about number and localization of both flows and cones is crucial as input for lava flow inundation models such as DOWNFLOW or Q–LavHA. The arising uncertainties were evaluated by Tarquini and Favalli [2013]. They found that random removal of 20–60 % of information on vent locations results in changes of 10–17 % in the resulting hazard maps. The effect is significant but does not introduce abrupt changes to the maps. For Bioko, we assume that we included the majority of the larger monogenetic cones and vents although we can not rule out that small or heavily eroded cones may not have been detectable on the DEM. At a location like Bioko, an L-Band mission such as the planned TanDEM-L by the DLR or the Rose-L by the European Space Agency would overcome this limitation and allow reflectivity of the ground even in the densely vegetated basins of Bioko Island.

5.1.2 *Model parameters (Hc and L) and DEM resolution*

Q–LavHA allows parametric fine-tuning by comparison of simulated lava flows and the outlines of (recent) lava flows on a pre-eruptive topography (DEM). Since we do not have these for Bioko, our best approach to assess lava flow hazards was to simulate various scenarios for a range of input parameters, based on our observations. In order to build the hazard maps within a reasonable computing time frame, we had to make compromises regarding the vent spacing and number of simulated flows per vent (*N*).

Tarquini and Favalli [2013] evaluated the impact of a variable vent spacing parameter for the DOWNFLOW model at Mt. Etna. They concluded that a spacing below 500 m results in a relative deviation of the resulting maps in the range of 6–8 % with respect to their reference map, which had a spacing of 80 m. Furthermore, they find that this effect is compensated for at lower elevations. In Bioko, most of the cities, villages, and critical infrastructure are located in coastal regions, and thus the impact of the described effect is negligible.

Another parameter that affects the computational time is *N*. Mossoux et al. [2016] state that $N = 1500$ is sufficient in most scenarios to provide robust results. For the hazard map of Mt. Karthala, a value of $N = 500$ at a vent spacing of 90 m on a 90 m DEM has been found to be satisfactory [Mossoux et al. 2019]. Kervyn et al. [2024] created hazard maps for Mt. Nyamulagira and Mt. Nyiragongo with $N = 100$ and a vent spacing of 30 m on a 30 m DEM, after thoroughly testing each parameter. Here, we found that a vent spacing of 300 m and $N = 500$ is a good compromise, and allows reasonable computational time frames of 6–8 days per hazard map on a DEM with 12 m resolution.

As Tarquini and Favalli [2013] showed, the flow length parameter is the most critical parameter affecting probabilistic lava flow distribution. Typically, the length parameter is determined by the length of the most recent flows, which in turn is mostly controlled by effusion and cooling rates [Walker 1973; Harris and Rowland 2009]. Furthermore, a negative linear relationship of vent elevations has been postulated for volcanic systems such as Mt. Etna, Nyiragongo, and Mt. Cameroon [Favalli et al. 2005; 2009a; b; 2012]. As Chevrel et al. [2021] showed for Piton de la Fournaise, this relationship does not hold true for every volcanic system. For the volcanoes on Bioko, we have insufficient data to test this relationship. We identified six relatively short flows but there is no information available on their ages. However, we have the age and location for the 1923 eruptive vent, which produced a lava flow of approximately 12 km. Other flows that may have reached the sea were not identifiable on the DEM, but field outcrops confirm that past flows have indeed reached

the coastline. Based on these observations, we argue that the short lava flows visible on the DEM were likely more viscous, making them thicker and more prominently expressed in the dataset. In contrast, longer flows, such as the 1923 flow, may have been thinner or channelized into erosional incisions, rendering them unrecognizable on the DEM.

Furthermore, basaltic magmas along the CVL (e.g. Mt. Cameroon and Pico Basilé) have similar geochemistry [Yamgouot et al. 2015], and thus potentially similar thermo-rheological properties [Wantim et al. 2013]. Compositionally, the erupted lavas at Mt. Cameroon [Déruelle et al. 2000; Suh et al. 2003] are quite similar to the compositions of the eruptive products of the volcanoes on Bioko [Yamgouot et al. 2015; 2016]. Mt. Cameroon being the closest and most active volcano along the CVL with respect to the volcanoes on Bioko, we argue that lava flow geometry statistics for Mt. Cameroon can be used as a first-order approximation for volcanoes on Bioko. Bonne et al. [2008] mapped a total of 42 lava flows at Mt. Cameroon with an average length of 4.4 km, but older and longer flows are likely to be obscured by vegetation and in turn biasing the inventory in favor of shorter flow lengths. The most recent six lava flows, which erupted between 1909 and 2000, ranged from 6.2 to 9.5 km with an average of 7.6 km [Favalli et al. 2012]. This is very similar to and hence supports our assumption to use an averaged length parameter of L = 7.5 km for the presented reference hazard map for Bioko (Figure 5).

Ideally, the length parameter and the elevation corrective factors (Hc and Hp) should be determined from the comparison of model-generated lava flow on a pre-eruptive DEM and the actual lava flow outline [Favalli et al. 2005; Chevrel et al. 2021]. However, as we discussed in the last paragraph, we do not have that information. Mossoux et al. [2016] suggests that, in absence of further information, the best approximation can be achieved by estimating an average flow thickness based on measurements in the field. During our fieldwork campaign, we measured the thickness of several lava flows and constrained Hc to 2–8 m, accordingly. Regarding the aforementioned similarities of the composition and source of lavas at Mt. Cameroon and the volcanoes on Bioko, we argue that the lavas for both systems are within similar rheology, and hence thickness ranges. The last six lava flows at Mt. Cameroon, erupted between 1909 and 2000, ranged from 0.7 to 12.7 m in thickness [Wantim et al. 2010; Favalli et al. 2012; Wantim et al. 2013], with an average of 4.9 m. This comparison supports our assumption of an averaged elevation corrective factor of Hc = 5 m for the presented reference hazard map for Bioko (Figure 5).

The optimal choice of elevation corrective factors also depends on the DEM resolution. As `Q-LavHA` distributes the simulated lava from pixel to pixel, the lava flows on a coarser DEM (e.g. 100 m, Figure 8B) are covering a larger area as the flows on a finer DEM (e.g. 12 m, Figure 8A). Despite the differences in the area covered by the simulated flows, the general behavior of the flows is similar. For the simulated vent at the summit of Pico Basilé (Figure 8), the flows are being blocked and redirected by the graben fault and then the majority is channelized into erosional incisions, independently of the DEM resolution. Tarquini and Favalli [2015] tested the sensitivity of flows simulated with `DOWNFLOW` to changes in the topographic resolution for well documented flows on Mt. Etna. They conclude that, if the pixel size effect is compensated (e.g. by resampling), the smoothing due to the decrease of topographic information has an almost negligible effect on how well simulated and real flows fit.

For multi-volcano hazard maps, the length parameter and elevation corrective factor should ideally be constrained for each individual volcano. As Kervyn et al. [2024] show, these parameters can vary, even for volcanoes that are located close to each other, such as Mt. Nyamulagira and Mt. Nyiragongo. Given the fact that there were no eruptions that produced lava flows on Bioko over the last decades that allowed for parametric fine-tuning for any of the three volcanoes on Bioko, and that data on other parameters such as flow length and thickness are also scarce, we argue that the reference hazard map (Figure 5) based on averaged input parameter for all three volcanoes, represents the best solution to assess the lava flow hazards until further data are available.

5.1.3 *Probability of vent opening*

The eruption probability distribution may vary from volcano to volcano as well. As a standard procedure, the vent density is used as an indicator for future vent opening probabilities based on the assumption that every new eruption forms a new vent with a clear morphological expression and that all vents have the same preservation potential [Connor et al. 2012; Connor et al. 2019]. However, vents may be masked by subsequent lava flows or covered by pyroclastic material from later eruptions in the vicinity. This is true in particular in areas of high vent densities, such as the rift zones along the long axis of Pico Basilé. This implies that vent opening probabilities in high vent densities areas are likely underestimated. Furthermore, our results show that the summits of Pico Biaó and Gran Caldera de Luba show only low probabilities of lava flow invasion. Although no monogenetic cones were observed inside the calderas and craters, it is likely that they were eruptive centers in the past and might be again in the future. Furthermore, the summit depression at Pico Biaó contains a crater lake and thus vent features are not detectable by radar. The PDF, and thus the resulting hazard maps, do not account for that properly and the hazards in the summit areas of both volcanoes is probably higher. In conclusion, the presented PDF probably underestimates the vent opening probability for the volcano's summit areas, and in particular, the rift zones with high vent densities. In turn, the vent opening probabilities for the areas with low vent densities are overestimated since the PDF is normalized to 1. This also implies slightly lower lava flow inundation probabilities for the downslope areas and in particular the coastal areas where most of the cities, villages, and infrastructure is located.

Another uncertainty arises from the lack of age data and thus eruption frequencies. Assuming that the relative vent density informs about the relative frequency of future eruptions between the three volcanoes is a large simplification. Systematic dating of eruption products would be required to further constrain the eruptive frequencies for each of the three

volcanoes to create a more realistic estimate on vent opening probabilities. In fact, there are indicators, such as the reports of the 1923 eruption and steam event at Pico Basilé, which allow the assumption that Pico Basilé is probably the most active of the three volcanoes. Although further data would be desirable, the highest vent opening probabilities are already indicated for the area south of the summit and parts of the summit itself of Pico Basilé.

5.2 Controls on lava flow pathways

The pathway of a lava flow is initially controlled by the location of the eruptive center. On Bioko, vents are clustering along the long axis of Pico Basilé, and the saddles between Pico Biaó and the other two volcanoes. These observations correspond with the accumulations of monogenetic cones and the vent opening probabilities as calculated for the PDF (Figure 4). Accordingly, the south of the summit of Pico Basilé shows intermediate lava inundation probabilities (Figure 5).

Lava flow pathways are mainly controlled by the topography and gravity. However, the viscosity and the correlated thickness of a lava flow defines the ability to surmount obstacles. With increasing the flow elevation corrective factor that acts as a proxy for flow thickness, larger topographic obstacles can be overcome. On Bioko, topographical controls include structural and erosional features such as faults and erosional gullies. In addition, pre-existing monogenetic cones act as obstacles. In areas of high cone densities, such as the rift zones, the simulated flows not only circumvent these cones but also are often confined by adjacent cones. For all simulated scenarios, the erosional incisions show the highest lava inundation probabilities. However, with an increasing flow elevation corrective factor, flows are being less easily channelized in gullies, and thus more likely to inundate adjacent areas (Figure 7). The process of lava flows filling up erosional incisions is known from other volcanoes such as Mt. Etna [Branca 2003]. For highly active volcanoes, which are often the best-studied volcanoes in terms of lava hazards, lava flows tend to level out erosional effects relatively quickly compared to less active volcanoes such as those on Bioko. In fact, the flanks of the three volcanoes on Bioko, and in particular the coastal regions are incised by deeply erosional processes (Figure 1). Therefore, we argue that the effects of erosional processes might have a greater potential impact on lava flow pathways on less active volcanoes. The main volcano-tectonic elements are the NE–SW-striking graben faults at the summit of Pico Basilé, and the complexly patterned faults around the summit of Pico Biaó (Figure 5). These faults redirect modeled lava flows pathways, possibly protecting large areas that would otherwise be downslope of a given vent, but also increasing the probabilities of other areas being inundated by lava (see Section 4.4). A similar pattern of lava flow inundation probability distribution can be observed for Mt. Cameroon. At Mt. Cameroon, the NE–SW striking graben faults are less pronounced, but still the northwestern and southeastern flanks show low inundation probabilities compared to the complementary sectors [Favalli et al. 2012]. In general, the channeling effect of volcano-tectonic structures is a common feature on other volcanoes. For example, it has been demonstrated that the rims of collapse structures, such as the Valle del Bove (Mt. Etna), the Enclos Fouqué (Piton de la Fournaise), and the Chã das Caldeiras (Fogo) have a noticeable influence on simulated lava flow pathways [Favalli et al. 2009b; Richter et al. 2016; Chevrel et al. 2021].

Regarding the ability of flows to overcome such structural obstacles, we tested which flow elevation corrective factors (Hc) would be necessary to overcome the eastern graben segment at the summit of Pico Basilé (Figure 7). We found that simulated flows with $H > 20$ m are able to overcome the fault. However, the randomized perturbation of the flow path inherent to the model introduced unrealistic flow pathways overcoming the graben fault regarding the fact that it has an offset of 50–70 m (Figure 7D). It is necessary to note that the majority of simulated flows with $Hc = 20$ m still followed the expected steepest pathways (Figure 7D).

6 Conclusions

The abundance of volcanic vents and outcrops of fresh lava flows as well as the CO_2 emissions on Bioko Island indicates that the volcanic system remains active and thus presents hazards for the island's communities from likely future eruptions. The primary volcanic hazard from these volcanoes is lava flow inundation. To assess lava flow hazards, we used Q–LavHA to build hazard maps for potential future eruptions on Bioko. We gathered vents and lava flows inventory and determined the main input parameters for Q–LavHA, the flow length and elevation corrective factor of the lava flow, based on observations on the TerraSAR-X and TanDEM-X DEM and during fieldwork. Our observations show that for the 7 mapped lava flows on Bioko, lengths range from 1.9 to 4.0 km, but sometimes may be long enough to reach the sea (~12 km), as may have occurred during the last eruption in 1923. We were able to identify the most likely vent location of the 1923 eruption based on comparison of flow simulations from different vents. During a field campaign, we observed lava flows of approximately 2 m to 8 m thickness. Furthermore, we mapped 436 eruptive vents on Bioko and calculated a Nearest Neighbor Index of 0.48, confirming a non-random, clustered distribution. Based on the vent locations, we calculated a kernel density estimation to assess the spatial variation of future vent opening probabilities. The highest probabilities are located along the main rift zones, in NE–SW at the long axis of Pico Basilé as well as the E–W-oriented saddle between Pico Biaó and Gran Caldera de Luba.

We present the first lava flow hazard map for Bioko and we highlight the importance of faults and structures in controlling the flow paths. We tested the effect of increasing lava flow length and flow elevation corrective factor, showing that more distal areas might be invaded by lava, and that larger obstacles can be overcome. The most likely lava pathways follow erosional incisions, but this confining effect becomes less effective with increasing flow thickness. We also show that in some places, lava flows are blocked or redirected by structural features, such as the graben faults at the summit of Pico Basilé or the complexly patterned faults around Pico Biaó.

Important infrastructure, like the capital Malabo, are located in coastal areas with relatively low lava invasion probabilities,

except for settlements like Lubá located at the outlet of an erosional gully north of Gran Caldera de Luba. This study provides the first long-term lava flow hazard map that may help for future volcanic crises management but future detailed risk assessment must be conducted.

Author Contributions

JB, LV, MOC, and TRW contributed to the conceptualization of the manuscript. TRW contributed to the satellite and structural analysis. JB, CRS, OANE planned and conducted the fieldwork campaign. JB wrote the manuscript, with supervision of MOC, TRW, and LV. MOC, TRW, CRS, OANE, and LV reviewed and edited the manuscript.

Acknowledgements

We acknowledge the provided datasets from the German Aerospace Center (DLR, 2021) based on the proposal DEM_GEOL3419. This work is part of the dissertation project of Jacob Brauner and therefore the general support of Drexel University and the members of the dissertation committee is greatly appreciated. We also want to thank the participants of the fieldwork campaign: Guillaume Boudoire, our drivers, as well as our friends and partners from the Bioko Biodiversity Protection Program and the Universidad Nacional de Guinea Ecuatorial, namely David M. Montgomery, Maximiliano F. Meñe, and Francisco M. Micha. This is contribution n°661 of the ClerVolc program of the International Research Center for Disaster Sciences and Sustainable Development of the University Clermont Auvergne. We would also like to thank Matthieu Kervyn and the anonymous reviewer for their thorough and constructive reviews, whose comments contributed significantly to the improvement of the manuscript.

Data Availability

All of our data, code, protocols, and in particular, the maps are available at www.zenodo.org in the repository https://doi.org/10.5281/zenodo.14920036.

Copyright Notice

References

Aka, F. T., K. Nagao, M. Kusakabe, H. Sumino, G. Tanyileke, B. Ateba, and J. Hell (2004). "Symmetrical Helium isotope distribution on the Cameroon Volcanic Line, West Africa". *Chemical Geology* 203(3–4), pages 205–223. DOI: 10.1016/j.chemgeo.2003.10.003.

Bebbington, M. S. (2013). "Assessing spatio-temporal eruption forecasts in a monogenetic volcanic field". *Journal of Volcanology and Geothermal Research* 252, pages 14–28. DOI: 10.1016/j.jvolgeores.2012.11.010.

Becerril, L., P. Larrea, S. Salinas, S. Mossoux, D. Ferrés, E. Widom, C. Siebe, and J. Martí (2021). "The historical case of Paricutin volcano (Michoacán, México): challenges of simulating lava flows on a gentle slope during a long-lasting eruption". *Natural Hazards* 107(1), pages 809–829. DOI: 10.1007/s11069-021-04607-x.

Bonne, K., M. Kervyn, L. Cascone, S. Njome, E. Van Ranst, E. Suh, S. Ayonghe, P. Jacobs, and G. Ernst (2008). "A new approach to assess long-term lava flow hazard and risk using GIS and low-cost remote sensing: the case of Mount Cameroon, West Africa". *International Journal of Remote Sensing* 29(22), pages 6539–6564. DOI: 10.1080/01431160802167873.

Branca, S. (2003). "Geological and geomorphological evolution of the Etna volcano NE flank and relationships between lava flow invasions and erosional processes in the Alcantara Valley (Italy)". *Geomorphology* 53(3–4), pages 247–261. DOI: 10.1016/s0169-555x(02)00315-x.

Brauner, J., T. R. Walter, O. A. N. Ela, and L. Vanderkluysen (2024). "Volcano-tectonic controls on the morphology and volcanic rift zone configuration on Bioko Island (Equatorial Guinea) derived from TanDEM-X data". *Bulletin of Volcanology* 86(8). DOI: 10.1007/s00445-024-01764-2.

Cappello, A., G. Bilotta, and G. Ganci (2022). "Modeling of Geophysical Flows through GPUFLOW". *Applied Sciences* 12(9), page 4395. DOI: 10.3390/app12094395.

Cappello, A., A. Hérault, G. Bilotta, G. Ganci, and C. Del Negro (2015a). "MAGFLOW: a physics-based model for the dynamics of lava-flow emplacement". *Geological Society, London, Special Publications* 426(1), pages 357–373. DOI: 10.1144/sp426.16.

Cappello, A., V. Zanon, C. Del Negro, T. J. L. Ferreira, and M. G. P. S. Queiroz (2015b). "Exploring lava-flow hazards at Pico Island, Azores Archipelago (Portugal)". *Terra Nova* 27(2), pages 156–161. DOI: 10.1111/ter.12143.

Cashman, K. V., C. Thornber, and J. P. Kauahikaua (1999). "Cooling and crystallization of lava in open channels, and the transition of Pāhoehoe Lava to 'A'ā". *Bulletin of Volcanology* 61(5), pages 306–323. DOI: 10.1007/s004450050299.

Chevrel, M. O., M. Favalli, N. Villeneuve, A. J. L. Harris, A. Fornaciai, N. Richter, A. Derrien, P. Boissier, A. Di Muro, and A. Peltier (2021). "Lava flow hazard map of Piton de la Fournaise volcano". *Natural Hazards and Earth System Sciences* 21(8), pages 2355–2377. DOI: 10.5194/nhess-21-2355-2021.

Chevrel, M. O., T. Platz, E. Hauber, D. Baratoux, Y. Lavallée, and D. Dingwell (2013). "Lava flow rheology: A comparison of morphological and petrological methods". *Earth and Planetary Science Letters* 384, pages 109–120. DOI: 10.1016/j.epsl.2013.09.022.

Connor, C. B. and L. J. Connor (2009). "Estimating spatial density with kernel methods". *Volcanic and Tectonic Hazard Assessment for Nuclear Facilities*. Cambridge University Press, pages 346–368. ISBN: 9780511635380. DOI: 10.1017/cbo9780511635380.015.

Connor, C. B., L. J. Connor, A. Germa, J. Richardson, M. Bebbington, E. Gallant, and A. Saballos (2019). "How to use ker-

nel density estimation as a diagnostic and forecasting tool for distributed volcanic vents". *Statistics in Volcanology* 4, pages 1–25. DOI: 10.5038/2163-338x.4.3.

Connor, L. J., C. B. Connor, K. Meliksetian, and I. Savov (2012). "Probabilistic approach to modeling lava flow inundation: a lava flow hazard assessment for a nuclear facility in Armenia". *Journal of Applied Volcanology* 1(1). DOI: 10.1186/2191-5040-1-3.

de' Michieli Vitturi, M. and S. Tarquini (2018). "MrLavaLoba: A new probabilistic model for the simulation of lava flows as a settling process". *Journal of Volcanology and Geothermal Research* 349, pages 323–334. DOI: 10.1016/j.jvolgeores.2017.11.016.

Del Negro, C., L. Fortuna, A. Herault, and A. Vicari (2008). "Simulations of the 2004 lava flow at Etna volcano using the magflow cellular automata model". *Bulletin of Volcanology* 70(7), pages 805–812. DOI: 10.1007/s00445-007-0168-8.

Déruelle, B., J. M. Bardintzeff, J. L. Cheminée, I. Ngounouno, J. Lissom, C. Nkoumbou, J. Étamé, J. V. Hell, G. Tanyileke, J. N'ni, B. Ateba, N. Ntepe, A. Nono, P. Wandji, J. Fosso, and D. G. Nkouathio (2000). "Simultaneous eruptions of basalt and hawaiite at Mt. Cameroon (28 March 17 April 1999)." *Comptes Rendus De L'Académie des Sciences Serie IIA - Sciences De La Terre Et Des Planetes* 331(8), pages 525–531.

Déruelle, B., I. Ngounouno, and D. Demaiffe (2007). "The 'Cameroon Hot Line' (CHL): A unique example of active alkaline intraplate structure in both oceanic and continental lithospheres". *Comptes Rendus. Géoscience* 339(9), pages 589–600. DOI: 10.1016/j.crte.2007.07.007.

Enciclopedia universal ilustrada europeo americana (1924). Barcelona: Hijos de J. Espasa. 833 pages.

Favalli, M., G. D. Chirico, P. Papale, M. T. Pareschi, and E. Boschi (2009a). "Lava flow hazard at Nyiragongo volcano, D.R.C.: 1. Model calibration and hazard mapping". *Bulletin of Volcanology* 71(4), pages 363–374. DOI: 10.1007/s00445-008-0233-y.

Favalli, M., F. Mazzarini, M. T. Pareschi, and E. Boschi (2009b). "Topographic control on lava flow paths at Mount Etna, Italy: Implications for hazard assessment". *Journal of Geophysical Research: Earth Surface* 114(F1). DOI: 10.1029/2007jf000918.

Favalli, M., M. T. Pareschi, A. Neri, and I. Isola (2005). "Forecasting lava flow paths by a stochastic approach". *Geophysical Research Letters* 32(3). DOI: 10.1029/2004gl021718.

Favalli, M., S. Tarquini, P. Papale, A. Fornaciai, and E. Boschi (2012). "Lava flow hazard and risk at Mt. Cameroon volcano". *Bulletin of Volcanology* 74(2), pages 423–439. DOI: 10.1007/s00445-011-0540-6.

Felpeto, A., V. Araña, R. Ortiz, M. Astiz, and A. García (2001). *Natural Hazards* 23(2/3), pages 247–257. DOI: 10.1023/a:1011112330766.

Grohmann, C. H. (2018). "Evaluation of TanDEM-X DEMs on selected Brazilian sites: Comparison with SRTM, ASTER GDEM and ALOS AW3D30". *Remote Sensing of Environment* 212, pages 121–133. DOI: 10.1016/j.rse.2018.04.043.

Harris, A. J. L. and S. K. Rowland (2009). "Effusion rate controls on lava flow length and the role of heat loss: a review". *Studies in Volcanology: The Legacy of George Walker*. Edited by T. Thordarson, S. Self, G. Larsen, S. K. Rowland, and Á. Höskuldsson. The Geological Society of London on behalf of The International Association of Volcanology and Chemistry of the Earth's Interior, pages 33–51. ISBN: 9781862392809. DOI: 10.1144/iavcel002.3.

Harris, A. J. L. and J. S. Allen (2008). "One-, two- and three-phase viscosity treatments for basaltic lava flows". *Journal of Geophysical Research: Solid Earth* 113(B9). DOI: 10.1029/2007jb005035.

Hedberg, J. D. (1969). "A geological analysis of the Cameroon trend". PhD thesis. Princeton University.

Herault, A., A. Vicari, A. Ciraudo, and C. Del Negro (2009). "Forecasting lava flow hazards during the 2006 Etna eruption: Using the MAGFLOW cellular automata model". *Computers & Geosciences* 35(5), pages 1050–1060. DOI: 10.1016/j.cageo.2007.10.008.

Hulme, G. (1974). "The Interpretation of Lava Flow Morphology". *Geophysical Journal International* 39(2), pages 361–383. DOI: 10.1111/j.1365-246x.1974.tb05460.x.

Instituto Geográfico Nacional (1981a). *Mapa de la Republica de Guinea Ecuatorial. Basacto del Oeste.* [Map scale 1:50,000]. URL: https://www.ign.es/web/BibliotecaIGN/20-A-20_01.jpg.

– (1981b). *Mapa de la Republica de Guinea Ecuatorial. Luba.* [Map scale 1:50,000]. URL: https://www.ign.es/web/BibliotecaIGN/20-A-20_03.jpg.

– (1981c). *Mapa de la Republica de Guinea Ecuatorial. Malabo.* [Map scale 1:50,000]. URL: https://www.ign.es/web/BibliotecaIGN/20-A-20_02.jpg.

– (1981d). *Mapa de la Republica de Guinea Ecuatorial. Riaba.* [Map scale 1:50,000]. URL: https://www.ign.es/web/BibliotecaIGN/20-A-20_04.jpg.

Kervyn, M., F. Barette, S. Poppe, B. Smets, A. Syavulisembo Muhindo, J. Kambale Makundi, Y. Ngunzi Kahashi, J. Kambale Ndagana, S. Mossoux, F. Kervyn, and C. Michellier (2024). "Assessing lava flow susceptibility at neighbouring volcanoes: Nyamulagira and Nyiragongo volcanoes, Virunga Volcanic Province". *Journal of Applied Volcanology* 13(1). DOI: 10.1186/s13617-024-00143-y.

Kubanek, J., J. A. Richardson, S. J. Charbonnier, and L. J. Connor (2015). "Lava flow mapping and volume calculations for the 2012–2013 Tolbachik, Kamchatka, fissure eruption using bistatic TanDEM-X InSAR". *Bulletin of Volcanology* 77(12). DOI: 10.1007/s00445-015-0989-9.

Le Corvec, N., K. B. Spörli, J. Rowland, and J. Lindsay (2013). "Spatial distribution and alignments of volcanic centers: Clues to the formation of monogenetic volcanic fields". *Earth-Science Reviews* 124, pages 96–114. DOI: 10.1016/j.earscirev.2013.05.005.

Marzoli, A., E. M. Piccirillo, P. R. Renne, G. Bellieni, M. Iacumin, J. B. Nyobe, and A. T. Tongwa (2000). "The Cameroon Volcanic Line Revisited: Petrogenesis of Continental Basaltic Magmas from Lithospheric and Asthenospheric Mantle Sources". *Journal of Petrology* 41(1), pages 87–109. DOI: 10.1093/petrology/41.1.87.

Moore, H. J., D. W. G. Arthur, and G. G. Schaber (1978). "Yield strengths of flows on the Earth, Mars, and Moon". *Proceedings of the 9th Lunar and Planetary Science Conference, Houston, TX*. Volume 3. A79-39253 16-91. ACM. New York, NY: Pergamon Press, Inc, pages 3351–3378.

Mossoux, S., M. Kervyn, and F. Canters (2019). "Assessing the impact of road segment obstruction on accessibility of critical services in case of a hazard". *Natural Hazards and Earth System Sciences* 19(6), pages 1251–1263. DOI: 10.5194/nhess-19-1251-2019.

Mossoux, S., M. Saey, S. Bartolini, S. Poppe, F. Canters, and M. Kervyn (2016). "Q-LAVHA: A flexible GIS plugin to simulate lava flows". *Computers & Geosciences* 97, pages 98–109. DOI: 10.1016/j.cageo.2016.09.003.

Njome, M. S. and M. J. de Wit (2014). "The Cameroon Line: Analysis of an intraplate magmatic province transecting both oceanic and continental lithospheres: Constraints, controversies and models". *Earth-Science Reviews* 139, pages 168–194. DOI: 10.1016/j.earscirev.2014.09.003.

Njome, M. S., C. E. Suh, R. S. J. Sparks, S. N. Ayonghe, and J. G. Fitton (2008). "The Mount Cameroon 1959 compound lava flow field: morphology, petrography and geochemistry". *Swiss Journal of Geosciences* 101(1), pages 85–98. DOI: 10.1007/s00015-007-1245-x.

Pedersen, G. B. M., M. A. Pfeffer, S. Barsotti, S. Tarquini, M. de'Michieli Vitturi, B. A. Óladóttir, and R. H. Þrastarson (2023). "Lava flow hazard modeling during the 2021 Fagradalsfjall eruption, Iceland: applications of MrLavaLoba". *Natural Hazards and Earth System Sciences* 23(9), pages 3147–3168. DOI: 10.5194/nhess-23-3147-2023.

Pinkerton, H. and L. Wilson (1994). "Factors controlling the lengths of channel-fed lava flows". *Bulletin of Volcanology* 56(2), pages 108–120. DOI: 10.1007/bf00304106.

Piper, J. D. A. and A. Richardson (1972). "The Palaeomagnetism of the Gulf of Guinea Volcanic Province, West Africa". *Geophysical Journal International* 29(2), pages 147–171. DOI: 10.1111/j.1365-246x.1972.tb02205.x.

Richter, N., M. Favalli, E. de Zeeuw-van Dalfsen, A. Fornaciai, R. M. da Silva Fernandes, N. M. Pérez, J. Levy, S. S. Victória, and T. R. Walter (2016). "Lava flow hazard at Fogo Volcano, Cabo Verde, before and after the 2014–2015 eruption". *Natural Hazards and Earth System Sciences* 16(8), pages 1925–1951. DOI: 10.5194/nhess-16-1925-2016.

Rizzoli, P., M. Martone, C. Gonzalez, C. Wecklich, D. Borla Tridon, B. Bräutigam, M. Bachmann, D. Schulze, T. Fritz, M. Huber, B. Wessel, G. Krieger, M. Zink, and A. Moreira (2017). "Generation and performance assessment of the global TanDEM-X digital elevation model". *ISPRS Journal of Photogrammetry and Remote Sensing* 132, pages 119–139. DOI: 10.1016/j.isprsjprs.2017.08.008.

Ryerson, F. J., H. C. Weed, and A. J. Piwinskii (1988). "Rheology of subliquidus magmas: 1. Picritic compositions". *Journal of Geophysical Research: Solid Earth* 93(B4), pages 3421–3436. DOI: 10.1029/jb093ib04p03421.

Schlund, M., M. M. Kotowska, F. Brambach, J. Hein, B. Wessel, N. Camarretta, M. Silalahi, I. N. Surati Jaya, S. Erasmi, C. Leuschner, and H. Kreft (2021). "Spaceborne height models reveal above ground biomass changes in tropical landscapes". *Forest Ecology and Management* 497, page 119497. DOI: 10.1016/j.foreco.2021.119497.

Schmidt, C., C. Laag, and J. Profe (2021). "Distribution of monogenetic volcanism along the Cameroon Line". *EGU General Assembly 2021 Abstracts*. EGU21-1755. Copernicus GmbH. DOI: 10.5194/egusphere-egu21-1755.

Schmidt, C., C. Laag, M. Whitehead, J. Profe, F. Tongwa Aka, T. Hasegawa, and G. Kereszturi (2022). "The complexities of assessing volcanic hazards along the Cameroon Volcanic Line using spatial distribution of monogenetic volcanoes". *Journal of Volcanology and Geothermal Research* 427, page 107558. DOI: 10.1016/j.jvolgeores.2022.107558.

Sealing, C. R. (2023). "Insights into the Magmatic System and Degassing Structures of Volcanoes on Bioko Island (Equatorial Guinea) from Fluid Geochemistry and Seismology". PhD thesis. Philadelphia: Drexel University.

Shaw, H. R. (1972). "Viscosities of magmatic silicate liquids; an empirical method of prediction". *American Journal of Science* 272(9), pages 870–893. DOI: 10.2475/ajs.272.9.870.

Suh, C. E., S. N. Ayonghe, R. S. J. Sparks, C. Annen, J. G. Fitton, R. Nana, and A. Luckman (2003). "The 1999 and 2000 eruptions of Mount Cameroon: eruption behaviour and petrochemistry of lava". *Bulletin of Volcanology* 65(4), pages 267–281. DOI: 10.1007/s00445-002-0257-7.

Tanase, M. A., I. Ismail, K. Lowell, O. Karyanto, and M. Santoro (2015). "Detecting and Quantifying Forest Change: The Potential of Existing C- and X-Band Radar Datasets". *PLOS ONE* 10(6). Edited by M. Jiang, e0131079. DOI: 10.1371/journal.pone.0131079.

Tarquini, S. and M. Favalli (2013). "Uncertainties in lava flow hazard maps derived from numerical simulations: The case study of Mount Etna". *Journal of Volcanology and Geothermal Research* 260, pages 90–102. DOI: 10.1016/j.jvolgeores.2013.04.017.

– (2015). "Simulating the area covered by lava flows using the DOWNFLOW code". *Geological Society, London, Special Publications* 426(1), pages 293–312. DOI: 10.1144/sp426.15.

Thierry, P., L. Stieltjes, E. Kouokam, P. Nguéya, and P. M. Salley (2008). "Multi-hazard risk mapping and assessment on an active volcano: the GRINP project at Mount Cameroon". *Natural Hazards* 45(3), pages 429–456. DOI: 10.1007/s11069-007-9177-3.

Tibaldi, A., F. Bonali, and C. Corazzato (2014). "The diverging volcanic rift system". *Tectonophysics* 611, pages 94–113. DOI: 10.1016/j.tecto.2013.11.023.

Vicari, A., H. Alexis, C. Del Negro, M. Coltelli, M. Marsella, and C. Proietti (2007). "Modeling of the 2001 lava flow at Etna volcano by a Cellular Automata approach". *Environmental Modelling & Software* 22(10), pages 1465–1471. DOI: 10.1016/j.envsoft.2006.10.005.

Walker, G. P. L. (1973). "Mount Etna and the 1971 eruption - Lengths of lava flows". *Philosophical Transactions of the Royal Society of London. Series A, Mathematical and Physical Sciences* 274(1238), pages 107–118. DOI: 10.1098/rsta.1973.0030.

Wantim, M., M. Kervyn, G. Ernst, M. del Marmol, C. Suh, and P. Jacobs (2013). "Numerical experiments on the dynamics of channelised lava flows at Mount Cameroon volcano with the FLOWGO thermo-rheological model". *Journal of Volcanology and Geothermal Research* 253, pages 35–53. DOI: 10.1016/j.jvolgeores.2012.12.003.

Wantim, M., C. Suh, G. Ernst, M. Kervyn, and P. Jacobs (2010). "Characteristics of the 2000 fissure eruption and lava flow fields at Mount Cameroon volcano, West Africa: a combined field mapping and remote sensing approach". *Geological Journal* 46(4), pages 344–363. DOI: 10.1002/gj.1277.

Wessel, B., M. Lachaise, M. Bachmann, B. Schweisshelm, M. Huber, T. Fritz, R. Tubbesing, and S. Buckreuss (2022). "The new TanDEM-X DEM 2020: generation and specifications". *EUSAR 2022; 14th European Conference on Synthetic Aperture Radar*. VDE, pages 1–5.

Yamgouot, F. N., B. Déruelle, I. B. Gbambié Mbowou, I. Ngounouno, and D. Demaiffe (2016). "Geochemistry of the volcanic rocks from Bioko Island ("Cameroon Hot Line"): Evidence for plume-lithosphere interaction". *Geoscience Frontiers* 7(5), pages 743–757. DOI: 10.1016/j.gsf.2015.06.003.

Yamgouot, F. N., B. Déruelle, I. B. G. Mbowou, and I. Ngounouno (2015). "Petrology of the Volcanic Rocks from Bioko Island ("Cameroon Hot Line")". *International Journal of Geosciences* 06(03), pages 247–255. DOI: 10.4236/ijg.2015.63019.